Geomechanics and Engineering, *Vol. 24, No. 5 (2021) 479-490*
DOI: https://doi.org/10.12989/gae.2021.24.5.479

Effects of the borehole drainage for roof aquifer on local stress in underground mining

Jianli Shao[1a], Qi Zhang*[2], Wenquan Zhang[1b], Zaiyong Wang[1] and Xintao Wu[1]

[1]*State Key Laboratory of Mining Disaster Prevention and Control Co-founded by Shandong Province and the Ministry of Science and Technology, Shandong University of Science and Technology, Qingdao 266590, China*
[2]*Department of Civil and Environmental Engineering, Stanford University, Stanford CA 94305, U.S.A.*

(Received September 7, 2020, Revised January 27, 2021, Accepted February 9, 2021)

Abstract. Pre-drainage of groundwater in the roof aquifer by boreholes is the main method for prevention of roof water disaster, and the drop in the water level during the drainage leads to the variation of the local stress in the overlying strata. Based on a multitude of boreholes for groundwater drainage from aquifer above the 1303 mining face of Longyun Coal Mine, theoretical analysis and numerical simulation are used to investigate the local stress variation in the process of borehole drainage. The results show that due to the drop in the water level of the roof aquifer during the drainage, the stress around the borehole gradually evolved. From the center of the borehole to the outside, a stress-relaxed zone, a stress-elevated zone, and a stress-recovered zone are sequentially formed. Along with the expansion of drainage influence, the stress peak in the stress-elevated zone also moves to the outside. When the radius of influence develops to the maximum, the stress peak position no longer moves outward. When the coal mining face advances to the drainage influence range, the abutment pressure in front of the mining face is superimposed with the high local stress around the borehole, which increases the risk of stress concentration. The present study provides a reference for the stress concentration caused by borehole drainage, which can be potentially utilized in the optimal arrangement of drainage boreholes in underground mining.

Keywords: mine water disaster; drainage; borehole; radius of influence; stress concentration

1. Introduction

As energy demand increases in China, the increasing mining depth and mining intensity aggravate the water inrush hazard (Sun *et al.* 2016, Zhao *et al.* 2020a). Water disaster in coal mine not only results in significant casualties and economic losses (Wang *et al.* 2018), but also aggravates the current situation of water shortage and negative ecological environment effect by unreasonable drainage (Hu *et al.* 2016, Loupasakis *et al*. 2014, Ma *et al.* 2019). Especially in the arid areas of Northwest China, the geological reserves of Jurassic coal resources account for about 60% of China's total coal resources. In the process of mining coal resources, roof water disasters such as flood of water, water inrush, and sand inrush continue to emerge, which has brought severe challenges to the prevention of mine water disasters and safety production.

Due to the complex geological conditions of most coal mines, China has been one of the most serious countries in the world for the mine water accidents (Wu *et al.* 2016, Zhao *et al.* 2020b, Zhou *et al.* 2020), and many mining operations are generally facing the threat of groundwater. When the mining-induced cracks spread into the roof aquifer, the groundwater flows indirectly or directly along the cracks, causing serious roof water disasters. For these mines with danger of water inrush in overlying confined aquifers, boreholes are usually carried out during tunneling to pre-drain groundwater in aquifers, directly or indirectly draining to the safe water head (See Fig. 1). This method reduces the threat of roof water hazards to mining operations and has become the most important preventive measure for roof water disasters in coal mines (Zhao *et al.* 2019a, Meng *et al.* 2018).

In order to ensure the effective drainage of the roof aquifer, coal enterprises usually design many boreholes for water exploration and drainage according to the conditions during tunneling. As an example, in the Jinjie Coal Mine of Shanxi province, China, pre-drainage of groundwater from aquifer have be arranged in 18 mining faces, and there are up to 146 drainage boreholes for a single working face. The pre-drainage water volume accounts for about 60% of the mine hydraulic discharge (Huang 2017). The first mining face of Caojiatan Coal Mine was arranged for 120 drainage boreholes. The project cost exceeded 5 million yuan, and water outflow of a single borehole could reach 80 m^3/h (Zhao *et al.* 2019a).

Based on numerous on-site drilling and drainage works, many scholars have summarized and analyzed the effects and laws of drilling drainage. Samani *et al.* (2006) derived the Laplace-transform solution for the problem of flow to horizontal drains in an anisotropic unconfined aquifer. Dong

*Corresponding author, Ph.D. Student
E-mail: qzhang94@stanford.edu
[a]Ph.D. Student
E-mail: shaojianli5020@163.com
[b]Professor
E-mail: wenquanzhang415@163.com

ISSN: 2005-307X (Print), 2092-6219 (Online)

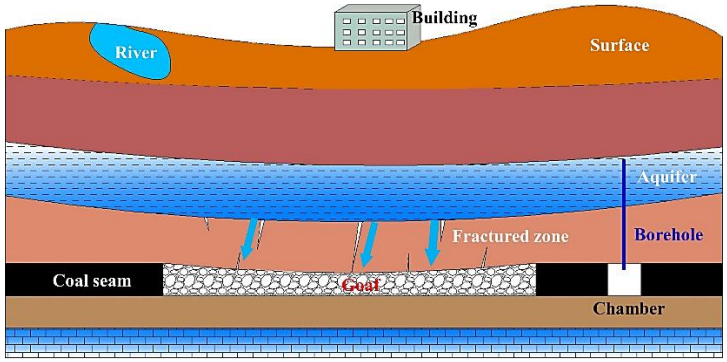

Fig. 1 Roof water inrush and the borehole drainage in underground mining

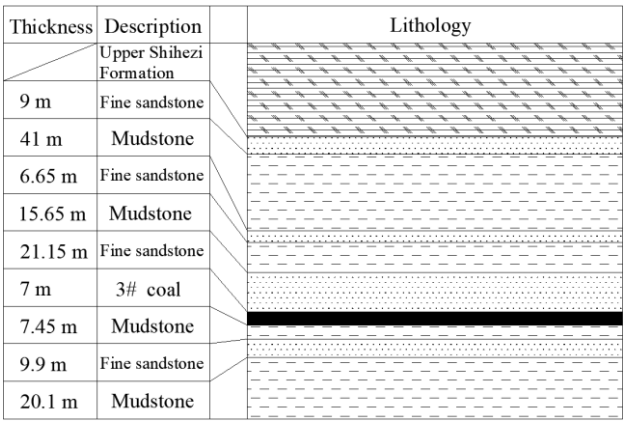

Fig. 2 Diagram of #3 coal seam and its roof and floor

et al. (2012) used the trial-and-error method to determine the satisfactory drainage capacity of an underground coal mine based on a calibrated numerical model. Yao (2011) hold the view that the roof water-rich stratum of roadway is rich in clay minerals, with well-developed intergranular pores and good connectivity, and its strength decreases in water, which are the internal factors of the intensity weakening for roadway wall rock.

The above-mentioned works provide references and basis for the aquifer drainage and the prevention of roof water disaster. However, from the perspective of rock mass stress-seepage coupling (Ahmed *et al.* 2019, Rongved and Cerasi 2019, Taleghani *et al.* 2018, Zhang 2020, Zhang *et al.* 2021), the changes in the water level and the radius of influence may cause local stress redistribution (Kim *et al.* 2018), and then have an impact on mining operations. The current studies in this area are not yet perfect. In this paper, we aim to establish a local borehole drainage model to analyze the variation of local stress during drainage, and then discuss the effects of the borehole drainage on the mining. According to the research results, it is suggested to consider the stress transfer effect in the process of drainage when arranging drainage boreholes, so as to reduce the stress concentration.

2. Engineering overviews

2.1 Geological and mining conditions

Longyun Coal Mine is located in the northernmost part of Juye Mine Field. The coal-bearing strata in the mine field are Shanxi Formation and Taiyuan Formation, and the main coal seam to be mined is 3# coal of Shanxi Formation. The depth of 1303 working face is between -1035 m to -933 m, and the average thickness of the coal seam is 7 m. According to the exploration data, the main aquifers developed from top to bottom in the working face include Quaternary, Neogene aquifer, Permian upper Shihezi Formation sandstone aquifer, and Permian Shanxi Formation sandstone aquifer. According to the spatial relationship between coal seam and aquifers, Quaternary and Neogene aquifers are separated by aquicludes with stable thickness and wide distribution. The possibility of infiltration of aquifer, atmospheric precipitation and surface water into deep aquifer is very small, which has no impact on mining activities in this mining area under normal conditions. Therefore, the roof aquifer that has great influence on the mining of #3 coal seam is mainly the sandstone aquifer of Shanxi Formation. The spatial relationship of roof strata is shown in Fig. 2.

2.2 Situation of water drainage in 1303 mining face

According to the high-density electrical measurement results of the mining face roof, there are 6 water-rich abnormal zones within the range of 60 m to 120 m of the roof of 1303 working face (as shown in Fig. 3). Combined with drilling analysis, the 6 water-rich areas are relatively stable in the range of 60 m to 120 m above the roof. Many boreholes were arranged for exploration and drainage

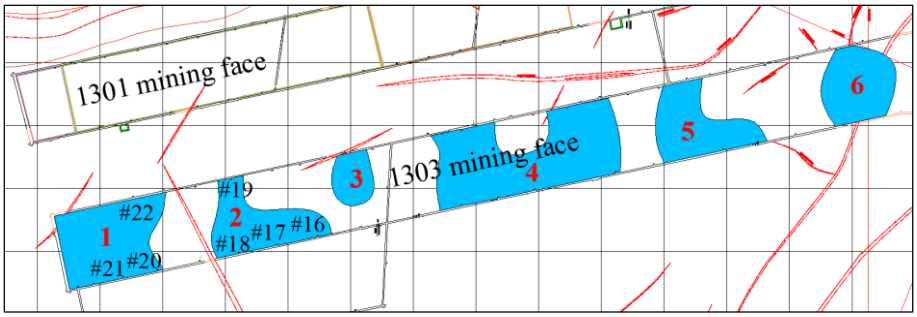

Fig. 3 Distribution of water-rich areas above 1303 mining face

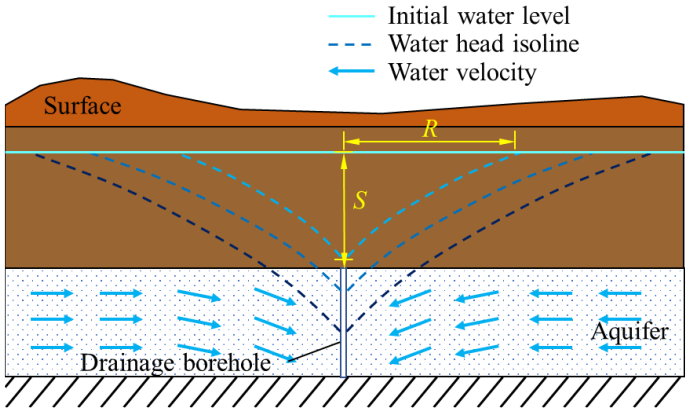

Fig. 4 Water head isoline and influence range of the borehole

before the 1303 working face mining. 314 boreholes were drilled into the sandstone aquifer of the Shanxi Formation, and the cumulative water discharge for all boreholes was 4344978 m^3 (during the tunneling). During the drainage, the maximum water outflow rate of a single hole was 94 m^3/h, and the maximum water pressure was 1.9 MPa for the borehole in #18 chamber. At present, the water discharge of this borehole is still maintained at about 50 m^3/h. The total outflow rate of the boreholes from #18 to #22 is about 150 m^3/h. After a great deal of drainage work of roof sandstone aquifer, the adjustment and redistribution of local stress caused by water level drop will inevitably have a certain impact on mining operations.

3. Local stress variation around drainage borehole

In this section, a simplified model of the borehole for water drainage from roof aquifer is established to analyzed the influence range and local stress variation during drainage.

3.1 Geological and mining conditions

At present, the flow of groundwater toward a fully penetrating well has been widely studied (Celik 2019, Feng *et al.* 2019). The following assumptions are generally adopted: 1) The roof aquifer is homogeneous and isotropic, with constant thickness, and horizontal and infinitely extending; 2) The water level of the roof aquifer before drainage is horizontal and stable; 3) The flow of water obeys Darcy's law.

According to the groundwater dynamics (Deng *et al.* 2019), in the stable stage, a cone-shaped depression zone is generally formed as a whole, which is called the cone of depression. The water head isoline and influence range of the borehole in stable stage are shown in Fig. 4. The water velocity, hydraulic gradient and influence range are expressed as follows:

$$v = KJ \tag{1}$$

$$J = \Delta H/\Delta S \tag{2}$$

$$R = r_0 + 10S\sqrt{K} \tag{3}$$

where, v is the flow velocity, m/s. K is the hydraulic conductivity, m/d. J is the hydraulic gradient. ΔH is the water head fall, m. ΔS is the distance of the water head isoline, m. R is the radius of influence, m. r_0 is the radius of the drainage borehole. S is the drop distance of water head in the borehole.

3.2 Seepage damage to rock

The flow of groundwater from aquifer to the borehole is essentially a transition of groundwater from slow seepage to pipeline flow, during which the velocity gradually increases (Li *et al.* 2019). In this process, on the one hand, the flow of water causes physical damage such as softening, scouring, particles migration and diffusion of cement and debris (Ji and Li 2018, Ma *et al.* 2017). On the other hand, cement

Table 1 The mechanical properties of the specimen damaged by different fluid velocity (Shu 2019)

	Compressive strength (MPa)	Tensile strength (MPa)	Elastic modulus (GPa)	Poisson's ratio	Internal friction angle (deg)	Cohesion (MPa)
Dry state	65	2.72	17	0.269	66.8	6.65
0 L/min	28.08	1.94	8.37	0.282	60.5	3.69
8 L/min	24.76	1.66	8.25	0.293	60.9	3.21
15 L/min	23.89	1.51	7.38	0.302	61.7	3.01

and debris continuously undergo chemical damage such as hydration, hydrolysis, corrosion, and redox in water (Feng and Ding 2007, Yasuhara *et al.* 2011). Kim *et al.* (2020) observed rapid tunnel over-displacement due to the squeezing of a fault rupture zone after the inflow of a large amount of groundwater. And upward infiltration pressure on the tunnel road was found to cause severe pavement damage. Shu (2019) studied the influence of different flow velocity on the mechanical properties of sandstone in water-rich area, such as friction angle, cohesion, tensile strength, and so on. The mechanical properties of the specimen weakened by water-rock interaction are shown in Table 1.

Considering the damage to the rock caused by long-term seepage of the borehole drainage in roof aquifer, the physical and mechanical parameters of the rock mass within the influence range are weakened after the initial stress balance of the model, and then the numerical computation is performed.

3.3 The mathematical model

3.3.1 Rock deformation

The assumption of small strain is adopted in this study. The mechanical equilibrium is described as follows:

$$\nabla \cdot \boldsymbol{\sigma} + \boldsymbol{F} = 0 \tag{4}$$

where, $\boldsymbol{\sigma}$ is the total stress tensor and $\boldsymbol{F}$ is the body force vector.

To take into account the coupling between rock deformation and pore fluid pressure, the classical Biot's poroelasticity theory is adopted here. Stress is positive during tension and negative during compression. The elastic effective stress tensor $\boldsymbol{\sigma}'$ is then defined by

$$\boldsymbol{\sigma}' = \boldsymbol{\sigma} + \alpha p \boldsymbol{m} \tag{5}$$

where, α is the Biot's coefficient, $\boldsymbol{m}$ is the second-order identity tensor, and p is the pore fluid pressure.

The strain tensor ε is related to the displacement vector via the kinematic compatibility relations

$$\boldsymbol{\varepsilon}(\boldsymbol{u}) = \frac{1}{2}\left[\nabla \boldsymbol{u} + (\nabla \boldsymbol{u})^{\mathrm{T}}\right] \tag{6}$$

where, $\boldsymbol{u}$ is the displacement vector.

3.3.2 Fluid flow in rock mass

As mentioned above, the rock is assumed to be an isotropic porous medium. The fluid flow in rock mass is described by mass conservation and Darcy's law:

$$\nabla \cdot (\rho \boldsymbol{v}) = 0 \tag{7}$$

$$\boldsymbol{v} = -\frac{k}{\mu}(\nabla p - \rho \mathbf{g}) \tag{8}$$

where, ρ is the fluid density. $\boldsymbol{v}$ is the fluid velocity. k is the permeability. μ is the fluid dynamic viscosity. $\mathbf{g}$ is the gravitational acceleration.

3.3.3 Permeability variation of rock mass

According to the cubic exponential relationship between permeability and porosity proposed by Palmer (2009) and Rutqvist and Tsang (2002), which can be written as:

$$k = k_0 \left(\frac{\phi}{\phi_0}\right)^3 \tag{9}$$

where, k_0 is the initial permeability. ϕ_0 is the initial porosity, and ϕ is the porosity.

The porosity of rock mass is related to stress state (Louis 1974), the follow relation is proposed:

$$\phi = (\phi_0 - \phi_{\mathrm{r}})\exp(\alpha_\phi \sigma_v) + \phi_{\mathrm{r}} \tag{10}$$

where, ϕ_{r} is the extreme porosity under high pressure, $\phi_{\mathrm{r}} \approx 0$. α_ϕ is the sensitivity coefficient of porosity with stress, $\alpha_\phi = 5.0 \times 10^{-8}\,\mathrm{Pa}^{-1}$ (Zhao *et al.* 2019b). σ_v is the average value of effective stress, which can be defined as follows:

$$\sigma_v = \frac{(\sigma_1 + \sigma_2 + \sigma_3)}{3} + \alpha p \tag{11}$$

where, σ_1, σ_2, and σ_3 are the maximum, the intermediate, and the minimum principal total stress, respectively.

3.3.4 Fluid flow in borehole

The drainage borehole is the outflow boundary of the aquifer seepage field. The borehole wall has hydraulic connection with the aquifer. Considering that the flow resistance in the drainage borehole is small and the borehole diameter is small, in order to maintain the size consistency between the borehole and the aquifer, the Darcy's law is amended as follows:

$$\nabla_{\mathrm{T}} \cdot (\rho \boldsymbol{v}_{\mathrm{b}} d_{\mathrm{b}}) = 0 \tag{12}$$

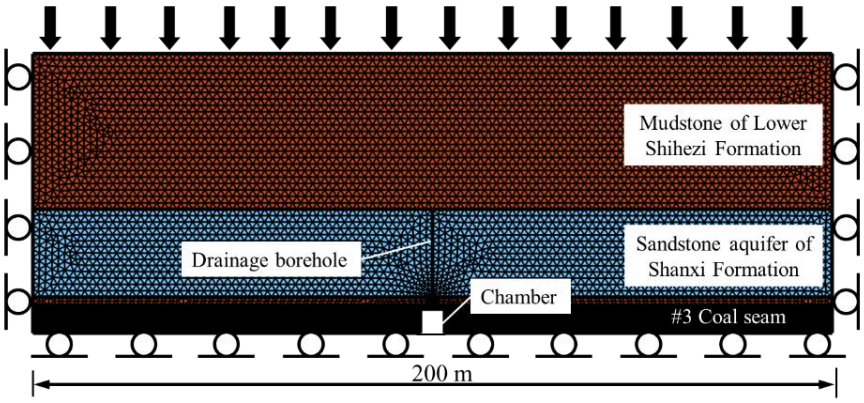

Fig. 5 Numerical model

Table 2 The mechanical properties used in the model

Lithology	Density (kg/m^3)	Elastic modulus (GPa)	Poisson's ratio	Initial porosity	Initial permeability (m^2)	Biot's coefficient
Mudstone	2600	3.55	0.26	0.15	4.5×10^{-9}	0.45
Sandstone aquifer	2380	3.12	0.28	0.24	7.8×10^{-8}	0.72
Mudstone	2600	3.55	0.26	0.16	4.5×10^{-9}	0.48
Coal	1400	3.25	0.32	0.18	8.0×10^{-9}	0.54
Borehole	/	/	/	/	0.0083	/

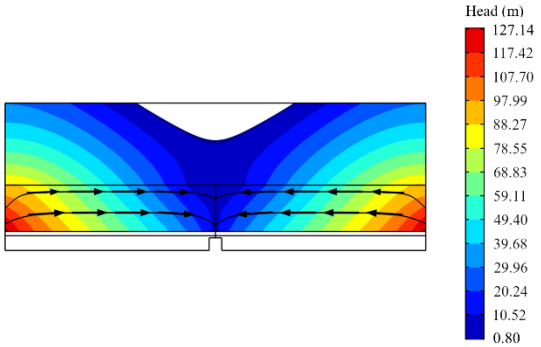

(a) 20 d

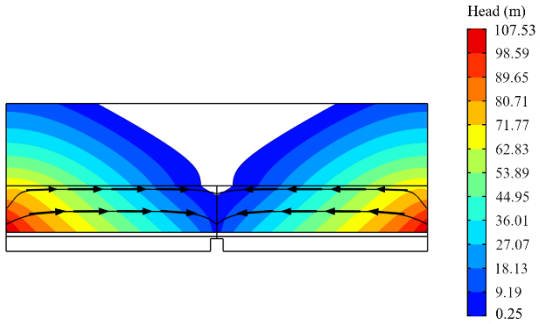

(b) 40 d

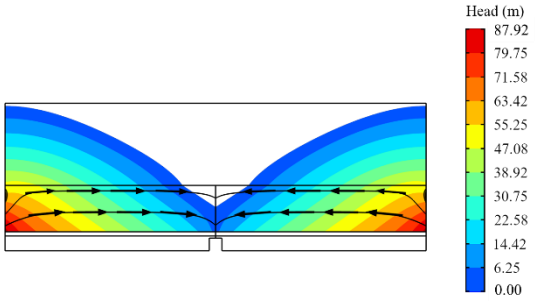

(c) 60 d

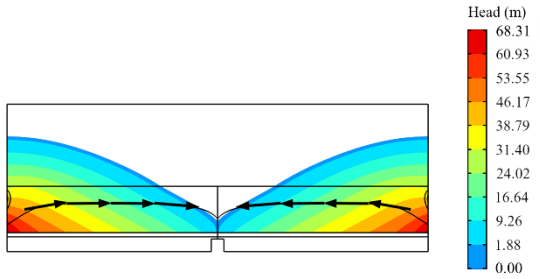

(d) 80 d

Fig. 6 Water head contours and streamlines during the drainage

$$\boldsymbol{v}_{\mathrm{b}} = -\frac{k_{\mathrm{b}}}{\mu}\left(\nabla_{\mathrm{T}} p - \rho \mathbf{g}\right) \tag{13}$$

where, d_{b} is the diameter of borehole. ∇_{T} is the gradient operator of the tangential plane of the borehole. $\boldsymbol{v}_{\mathrm{b}}$ is the flow velocity. k_{b} is the permeability of borehole, which can be expressed by the cubic law as follows (FiaFR 2020):

$$k_{\mathrm{b}} = \frac{d_{\mathrm{b}}^2}{12\,\mathrm{f}} \tag{14}$$

where, f is the borehole's friction factor (f = 1 is assumed in

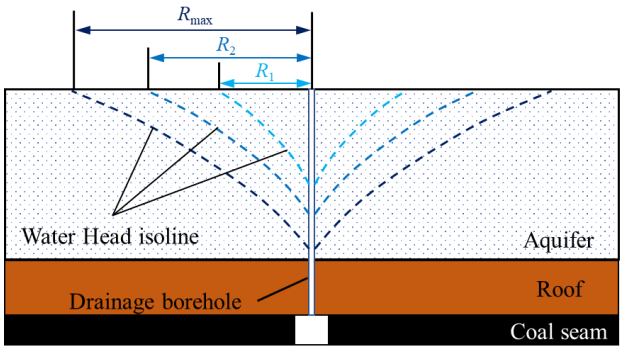

Fig. 7 Radius of influence during the borehole drainage

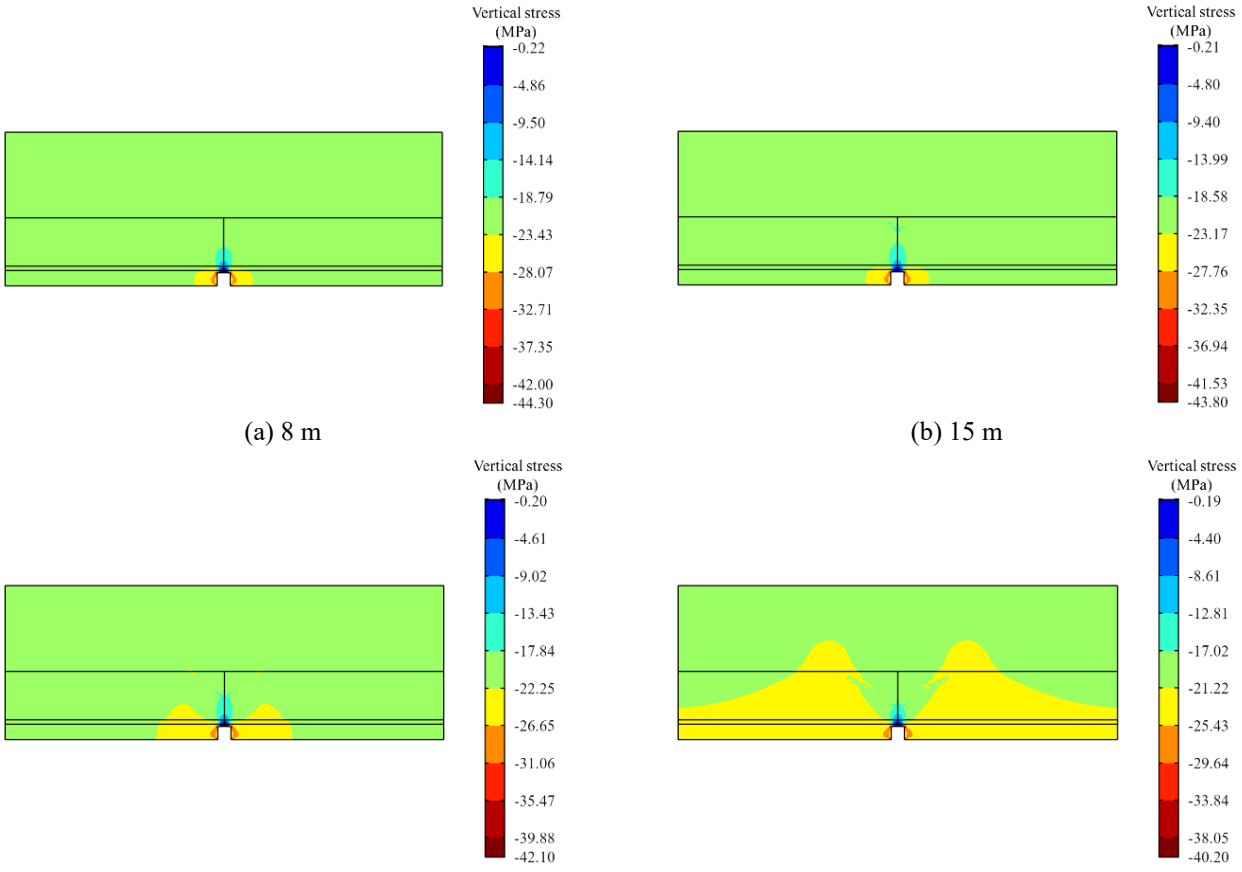

Fig. 8 Local vertical stress distribution with different radius of influence, note the vertical stress plotted in this work is component of the effective stress tensor $\boldsymbol{\sigma}'$

our study).

3.4 Numerical model

Taking the drainage chamber in roadway of 1303 mining face as a case, a numerical model is established, as shown in Fig. 5, which is based on the in-site lithological conditions illustrated in Fig. 2. The model is 200 m wide and 100 m high, and the drainage chamber is located in the horizontal center. The drainage borehole is located above the chamber and intersect the whole sandstone aquifer of Shanxi Formation on the roof.

The buried depth of coal seam is about -940 m. Vertical stress is used to simulate the overlying strata pressure (20 MPa) at the upper boundary. In the lateral boundaries, horizontal displacements are constrained. In the bottom boundary, the vertical displacements are constrained. The initial head of sandstone aquifer in Shanxi Formation is 200 m, which increases with the increase of depth. And the water head drops 10 m at each step, simulating the water head drop of the aquifer once every 5 days. The fracture flow node is added on boundaries to define the flow along interior boundaries representing the drainage borehole within rock mass. The bottom of the borehole is the outflow

boundary of the drainage borehole (zero pressure). Other boundaries are no flow.

To solve the coupled equations of stress and seepage fields, the commercial finite element software of COMSOL Multiphysics was used. High density and quality grids for the model were generated (a total of 9208 triangular elements) to guarantee sufficient accuracy and good iteration convergence in the COMSOL simulation. Table 2 summarizes the properties used in the model. Through this numerical model, the variation of water level in roof aquifer and stress around the borehole can be observed and analyzed.

3.5 Result analysis

3.5.1 Influence range during the drainage

The water pressure head contours and streamlines in the process of the borehole drainage are shown in Fig. 6. With the change of the water level, a cone-shaped depression zone around the borehole is formed in the aquifer, and the groundwater continuously seeps into the borehole from the aquifer. The simulation results are consistent with the theoretical analysis shown in Fig. 4. At the same time, the flow field coupling model of aquifer seepage and borehole pipe flow is realized.

As the water level continues to drop during the drainage, the cone-shaped depression zone expands outward, and its influence radius also increases. If there is a recharge source in the aquifer, when the volume of discharge is equal to the recharge, the cone-shaped depression zone will no longer expand outward, and there is a maximum influence radius $R_{\max} = r_0 + 10S\sqrt{K}$. Then, the influence radius variation during the drainage is summarized in Fig. 7. If there is no recharge source in the aquifer, the influence range will continue to expand outward. At this point, the maximum influence radius $R_{\max}$ is the distance between the borehole and the boundary of the water-rich area.

3.5.2 Local stress variation during borehole drainage

Fig. 8 shows the local vertical stress distribution when the radius of influence are 8 m, 15 m, 25 m, and 45 m, respectively. It can be seen from the figure that the local vertical stress around the borehole has changed significantly during the drainage. The area with the lowest vertical stress is always near the borehole center, and the higher vertical stress zone is outside the borehole. With the expansion of influence radius, the higher vertical stress zone around the borehole gradually expands outward.

The vertical stress curves in roof aquifer during drainage are plotted in Fig. 9. It is seen that the vertical stress in roof aquifer changes obviously. Compared with the undisturbed original stress of 20.9 MPa at a distance, the stress around the borehole decreases, while the stress on the edge of the influence radius increases. This outcome means that from the center of the borehole to the outside, a stress-relaxed zone, a stress-elevated zone, and a stress-recovered zone are sequentially formed. The peak stress is always located on the edge of the radius of influence, when the radius of influence extends, the peak stress and the stress-elevated zone gradually moves outward.

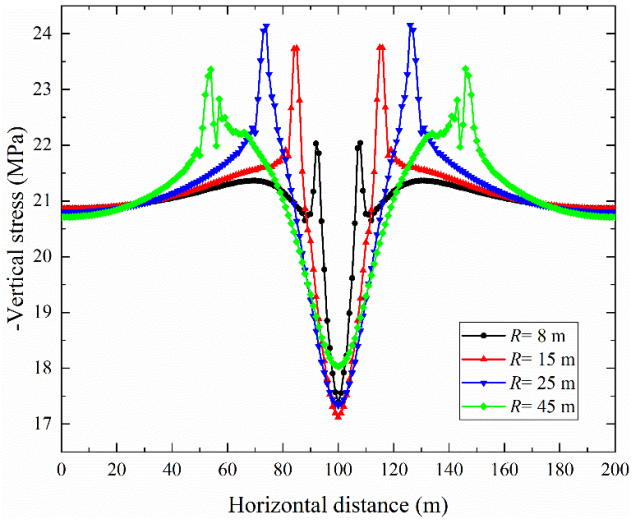

Fig. 9 Vertical stress distribution in roof aquifer with different radius of influence

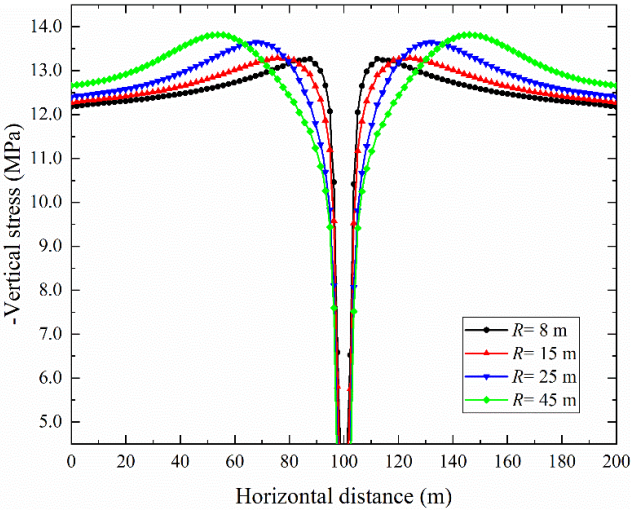

Fig. 10 Vertical stress distribution in coal roof with different radius of influence

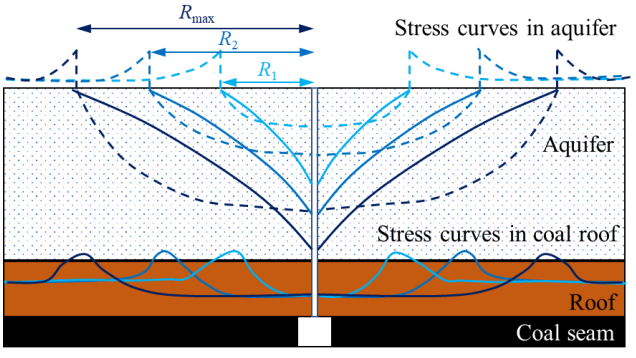

Fig. 11 Local stress variation during the drainage from roof aquifer

The vertical stress curves in coal roof during drainage are plotted in Fig. 10. Under the influence of the vertical stress variation of roof aquifer, the stress of coal roof also changes. Similarly, with the transfer of overburden stress,

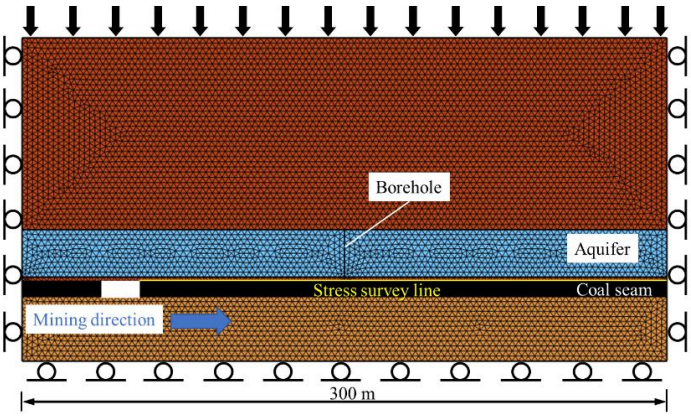

Fig. 12 Numerical model of mining advancing

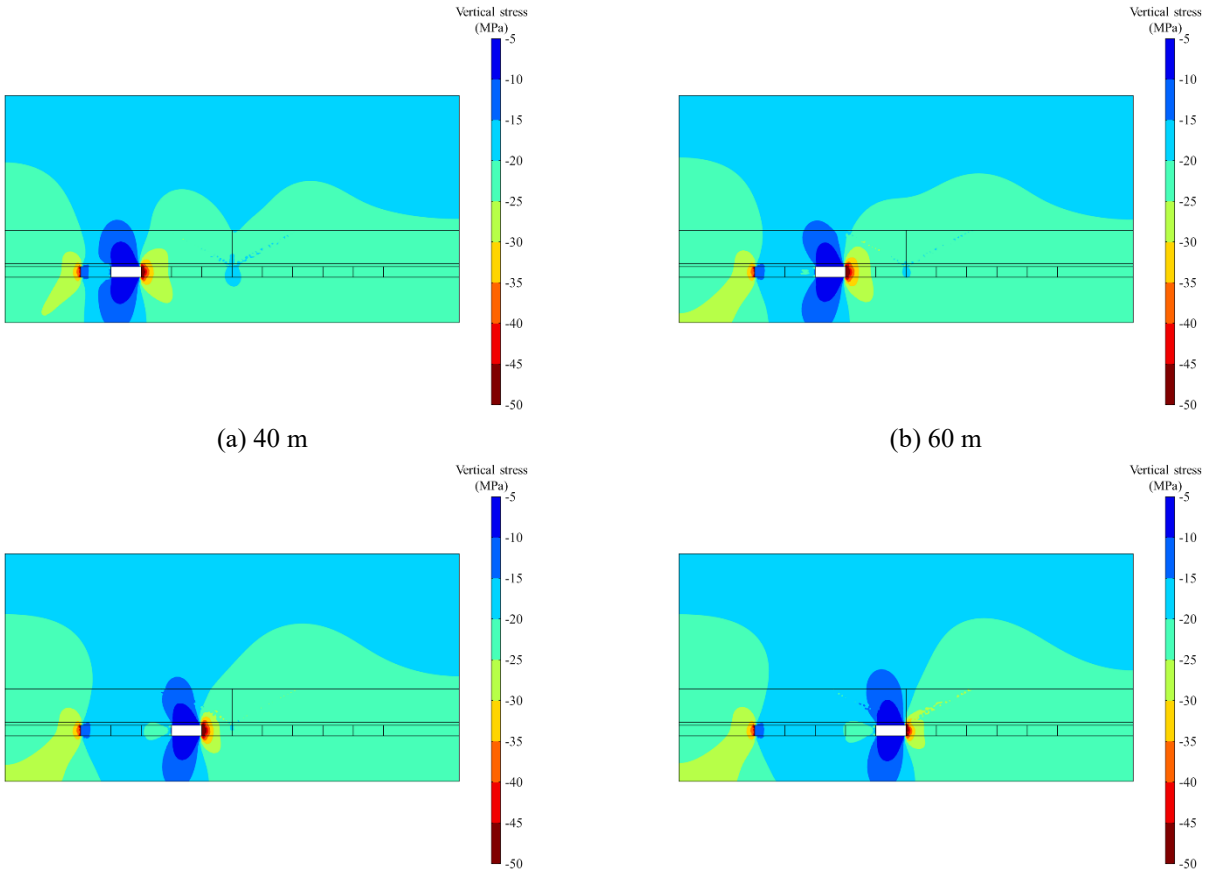

(a) 40 m (b) 60 m

(c) 80 m (d) 100 m

Fig. 13 Distribution of distribution of vertical stress during mining

the local stress of coal seam roof is differentiated. And the stress-relaxed zone and the stress-elevated zone also appear. With the influence radius extended, the peak stress in coal roof also moves to the outside. This indicates that the water drainage from roof aquifer by boreholes may cause the stress concentration in stratum.

Combined with the above analysis, the local stress is redistributed due to the borehole drainage. The borehole drainage for roof aquifer reduces the local vertical stress level. Then the stress shifts outward and redistributes, forming a vertical stress concentration at the influence radius. With the expansion of influence range, the position of stress concentration also moves outward continuously. When the influence range of drainage expands to a certain extent, there will be a fixed radius R_{max} in the influence range, and the stress concentration position will no longer move outward. Then the stress variation in the overburden during the drainage can be summarized in Fig. 11.

4. Impact of the drainage-induced stress variation on mining operations

After long-term drainage by the borehole, the influence range in roof aquifer above 1303 working face has become

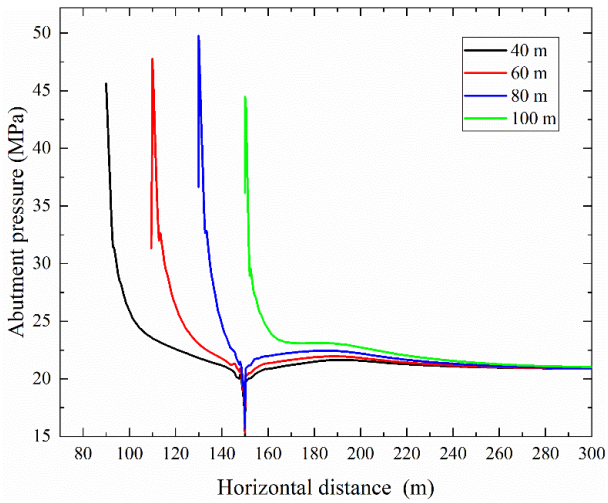

Fig. 14 Abutment pressure in front of the mining face during mining

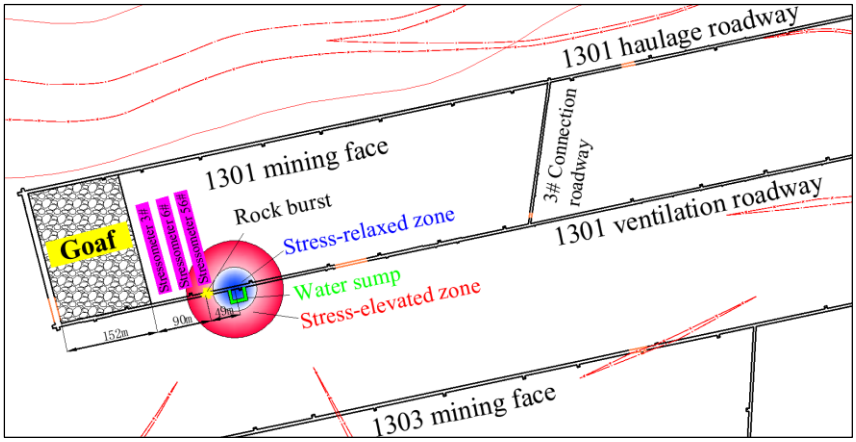

Fig. 15 Location of rock burst in adjacent 1301 working face

(a) Broken anchor net

(b) Floor heave

Fig. 16 Serious destroy in the roadway

stable. When the mining nears the influence range, it is easy to be affected by local stress of borehole drainage. This section discusses the impact of local stress variation around the drainage borehole on mining

4.1 Numerical model

As shown in Fig. 12, a simplified mechanical model is established in line with the engineering geological conditions of the 1303 mining face. The model size is 300 m wide and 200 m high. The drainage borehole is located in the horizontal center and intersects the whole sandstone aquifer of Shanxi Formation. A uniform load of 20 MPa is applied to the upper boundary of the model. The lateral boundaries are constrained by horizontal displacement, and the bottom boundary is constrained by vertical displacement. After long-term drainage, the water pressure of the aquifer tends to be stable, and the initial head in this model is set at 100 m. Consistent with the previous model, the borehole is set as the fracture flow boundary. The attributes in Table 2 are still input as model parameters. Similarly, high density and quality grids for this model were generated (a total of 13112 triangular elements) to guarantee sufficient accuracy and good iteration

convergence in the COMSOL simulation.

The open-off cut in the coal seam is 50 m away from the left boundary of the model, and each step is simulated to mining 20 meters until it reaches the place near the drainage hole. In order to reflect the actual situation of roof caving in goaf, the previous advancing section is filled every other advance to simulate the collapse and compaction of stope. Assuming that the influence range of drainage has been stable, stress survey line is arranged at the top of coal seam to analyze the change of abutment pressure in front of working face during mining.

4.2 Result analysis

The vertical stress in the domain during mining advancing is calculated and plotted in Fig. 13. When the excavation is 40 m, the peak abutment pressure is 45.76 MPa, and the stress concentration factor is 2.18. When the excavation is 60 m, the peak abutment pressure is 47.84 MPa, the stress concentration factor is 2.28. The stress concentration coefficient increases, and the ground pressure behavior is obvious in front of the mining face. When the excavation is 80 m, the peak abutment pressure is 49.26 MPa, and the stress concentration factor is 2.35. The stress concentration factor increases rapidly, and the impact risk is high. When the excavation is 100 m, the peak abutment pressure is 44.34 MPa, the stress concentration factor is 2.12, and the stress concentration factor decreases.

Fig. 14 depicts the abutment pressure in front of the working face during mining advancement. It can be seen that as the advancing of the mining face from 40 m to 80 m, the peak abutment pressure in front of the working face increases gradually. Combined with the analysis in section 3.5, this is due to that the mining face gradually enters the local stress-elevated zone of the drainage borehole, and the front abutment pressure and the local high stress of the drainage borehole superimpose to form a high stress concentration. However, as the mining face advances to the center of the drain borehole, the front abutment pressure peak decreases suddenly, which is affected by the local stress-relaxed zone of the drainage borehole. Far away in front of work, the abutment pressure gradually returns to the original rock stress. Consequently, the mining face is easy to be affected by the borehole drainage during mining advancing, especially the abutment pressure increases significantly near the influence radius, but decreases near the drainage borehole center.

The borehole drainage from roof aquifer leads to stress transfer, forming the local stress-elevated zone and stress-relaxed zone. And the coal in front of the working face has been in the limit equilibrium state under the high abutment pressure during mining advancing. When the front abutment pressure of the working face superposes the local stress-elevated zone of the borehole drainage, a high stress concentration is formed. When the strength of surrounding rock exceeds the limit, it will increase the risk of rock burst accident.

4.3 Validation by field data

Before mining in the adjacent 1301 working face, a great deal of drainage work has been done. Seven upward boreholes drained from the aquifer with a length of 55 m were arranged in the water sump. After 30 days of the drainage, the water pressure of the roof confined aquifer decreased to 0.1 ~ 0.4 MPa. By Eq. (3), the influence radius has reached about 40 m ~ 80 m. And according to the findings in the paper, there is a stress-elevated zone (See Fig. 15). When the 1301 mining face was excavated to 152 m, the Stressometer 56# (91 m away from the mining face) and Stressometer 6# (63 m away from the mining face) at the site increased by 3.2 and 4.5 MPa, respectively. It indicates that these stressometers are in the increased stress-elevated zone. But the Stressometer 3# (33 m away from the mining face) has remained unchanged. A serious rock burst occurred in the roadway of the 1301 working face (See Fig. 16), and the location of the rock burst was 90 m away from the working face. The accident position is just located in the local stress-elevated zone of the boreholes in water sump. The variations of field data are in good agreement with the results of this study. The high stress concentration is formed by the superposition of front abutment pressure and local high stress by the drainage (as shown in Fig. 17).

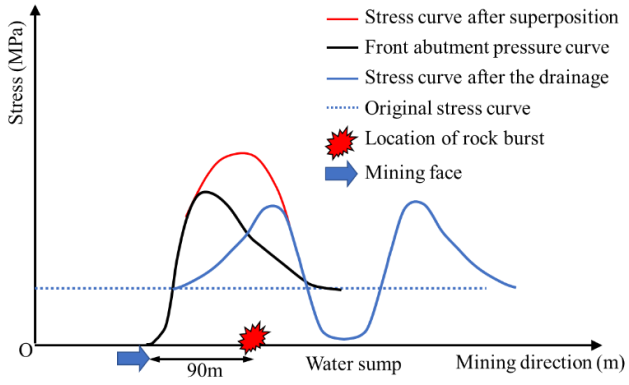

Fig. 17 Diagram of stress superposition in front of 1301 mining face

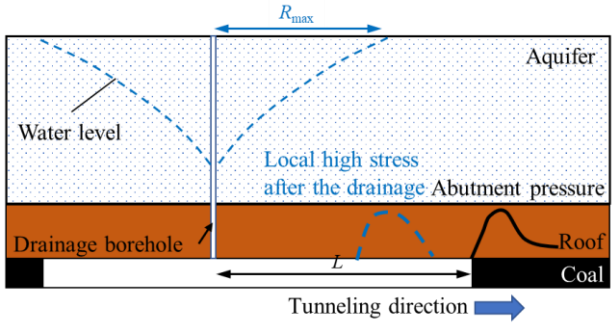

Fig. 18 Optimization for the borehole position during tunneling

During the drainage by boreholes, the peak stress in rock stratum continuously moves outward with the expansion of influence range. When the influence range of the drainage extends to R_{max}, the peak stress in with the expansion of drainage influence range will stop moving outward. In order to avoid the superposition of front

abutment pressure and local high stress caused by drainage, it is suggested that the distance L of drainage borehole behind the tunneling place should be greater than the maximum range of drainage influence R_{max}, as shown in Fig. 18. In addition, stress monitoring and early warning should be strengthened, and measures such as hydraulic fracturing and pressure relief by large-diameter boreholes should be taken in time to reduce the risk of stress concentration and ensure coal mining safety.

5. Conclusions

A stress-seepage coupled numerical model is established to investigate the local stress variation induced by the borehole drainage from roof aquifer, and the effects of the stress variation on the mining operations are further analyzed. The following conclusions are drawn:

• The borehole drainage results in the stress transfer of the roof aquifer, and the local stress-relaxed zone, the stress-elevated zone and the stress-recovered zone are formed from the borehole center to the outside. During the drainage, the influence range gradually expands, and the stress-elevated zone also gradually expands outward, until the influence radius extends to R_{max}, the stress-elevated zone stops moving.

• The front abutment pressure is usually caused by excavation. When the peak stress of local stress-elevated zone caused by drainage superimposes with the front abutment pressure, the high stress concentration is formed. However, for the coal seam which has been in the limit equilibrium state in front of the mining face, it is easy to induce rock burst accidents.

• For the local high stress caused by the drainage, the layout of boreholes should be optimized, stress monitoring should be strengthened and pressure relief measures should be taken to avoid superimposing with other stress concentration to ensure safety.

Conflicts of Interest

The authors declare that they have no conflicts of interest.

Acknowledgments

The research described in this paper was financially supported by the Natural Science Foundation (Grant Nos. 51774199 and 51974172), Natural Science Foundation of Shandong Province (Grant No. 2019MEE004).

References

Ahmed, E., Fumagalli, A. and Budiša, A. (2019), "A multiscale flux basis for mortar mixed discretizations of reduced Darcy-Forchheimer fracture models", *Comput. Method. Appl. Mech. Eng.*, **354**, 16-36. https://doi.org/10.1016/j.cma.2019.05.034.

Celik, F. (2019), "The observation of permeation grouting method as soil improvement technique with different grout flow models", *Geomech. Eng.*, **17**(4), 367-374. https://doi.org/10.12989/gae.2019.17.4.367.

Dong, D., Sun, W. and Xi, S. (2012), "Optimization of mine drainage capacity using FEFLOW for the No. 14 coal seam of China's Linnancang Coal Mine", *Mine Water Environ.*, **31**(4), 353-360. https://doi.org/10.1007/s10230-012-0205-5.

Deng, D.P., Li, L. and Zhao, L.H. (2019), "Stability analysis of slopes under groundwater seepage and application of charts for optimization of drainage design", *Geomech. Eng.*, **17**(2), 181-194. https://doi.org/10.12989/gae. 2019.17.2.181.

Feng, Q., Yuan, X. and Zhan, H. (2019), "Flow to a partially penetrating well with variable discharge in an anisotropic two-layer aquifer system", *J. Hydrol.*, **578**(124027). https://doi.org/10.1016/j.jhydrol.2019.124027.

Feng, X. and Ding, W. (2007), "Experimental study of limestone micro-fracturing under a coupled stress, fluid flow and changing chemical environment", *Int. J. Rock Mech. Min. Sci.*, **44**(3), 437-448. https://doi.org/10.1016/j.ijrmms.2006.07.012.

FiaFR (2020), Flow in a Fractured Reservoir 90421; COMSOL Inc. http://cn.comsol.com/model/flow-in-a-fractured-reservoir-90421.

Hu, Z.Q., Chen, C., Xiao, W., Wang, X.J. and Gao, M.J. (2016), "Surface movement and deformation characteristics due to high-intensive coal mining in the windy and sandy region", *Int. J. Coal Sci. Technol.*, **3**(3), 339-348. https://doi.org/10.1007/s40789-016-0144-z.

Huang, H. (2017), "Optimization research on dewatering technology of roof water in Jinjie mine", Ph.D. Dissertation, Graduate School of China Coal Research Institute, Beijing, China.

Ji, Y., and Li, X. (2018), "Analysis on Geo-stress and casing damage based on fluid-solid coupling for Q9G3 block in Jibei oil field", *Geomech. Eng.*, **15**(1), 677-686. https://doi.org/10.12989/gae.2018.15.1.677.

Kim, J., Kim, J., Lee, J. and Yoo, H. (2018), "Prediction of transverse settlement trough considering the combined effects of excavation and groundwater depression", *Geomech. Eng.*, **15**(3), 851-859. https://doi.org/10.12989/gae.2018.15.3.851.

Kim, N., Park, D., Jung, H. and Kim, M. (2020), "Deformation characteristics of tunnel bottom after construction under geological conditions of long-term deformation", *Geomech. Eng.*, **21**(2), 171-178. https://doi.org/10.12989/gae.2020.21.2.171.

Li, B., Fang, H., Yang, K., He, H., Tan, P. and Wang, F. (2019), "Mechanical response and parametric sensitivity analyses of a drainage pipe under multiphysical coupling conditions", *Complexity*, 3635621. https://doi.org/10.1155/2019/3635621.

Loupasakis, C., Angelitsa, V., Rozos, D. and Spanou, N. (2014), "Mining geohazards-land subsidence caused by the dewatering of opencast coal mines: The case study of the Amyntaio coal mine, Florina, Greece", *Nat. Hazards*, **70**(1), 675-691. https://doi.org/10.1007/s11069-013-0837-1.

Louis, C. (1974), Rock Hydraulics, in *Rock Mechanics*, Springer, Vienna, Austria.

Ma, D., Rezania, M., Yu, H. and Bai, H. (2017), "Variations of hydraulic properties of granular sandstones during water inrush: Effect of small particle migration", *Eng. Geol.*, **217**, 61-70. https://doi.org/10.1016/j.enggeo.2016.12.006.

Ma, D., Wang, J. and Li, Z. (2019), "Effect of particle erosion on mining-induced water inrush hazard of karst collapse pillar", *Environ. Sci. Pollut. R.*, **26**(19), 19719-19728. https://doi.org/10.1007/s11356-019-05311-x.

Meng, L., Feng, Q. and Li, Q. (2018), "Coupled simulation-optimization model for draining confined aquifer via underground boreholes to prevent water inrush of coal mines", *Environ. Earth Sci.*, **77**(17), 607.

https://doi.org/10.1007/s12665-018-7794-7.
Palmer, I. (2009), "Permeability changes in coal: Analytical modeling", *Int. J. Coal Geol.*, **77**(1-2), 119-126. https://doi.org/10.1016/j.coal.2008.09.006.
Rongved, M. and Cerasi, P. (2019), "Simulation of stress hysteresis effect on permeability increase risk along a fault", *Energies*, **12**(18), 3458. https://doi.org/10.3390/en12183458.
Rutqvist, J. and Tsang, C. (2002), "A study of caprock hydromechanical changes associated with CO_2-injection into a brine formation", *Environ. Geol.*, **42**(2-3), 296-305. https://doi.org/10.1007/s00254-001-0499-2.
Samani, N., Kompani-Zare, M., Seyyedian, H. and Barry, D.A. (2006), "Flow to horizontal drains in isotropic unconfined aquifers", *J. Hydrol.*, **324**(1-4), 178-194. https://doi.org/10.1016/j.jhydrol.2005.10.003.
Shu, C.X. (2019), "The mechanism and prevention of rock burst at the water-rich working face in the deep zone of mine in the adjacent area of Shaanxi and Inner Mongolia", Ph.D. Dissertation, University of Science and Technology Beijing, Beijing, China.
Sun, W.J., Zhou, W.F. and Jiao, J. (2016), "Hydrogeological classification and water inrush accidents in China's coal mines", *Mine Water Environ.*, **35**(2), 214-220. https://doi.org/10.1007/s10230-015-0363-3.
Taleghani, A. D., Gonzalez-Chavez, M., Yu, H., and Asala, H. (2018), "Numerical simulation of hydraulic fracture propagation in naturally fractured formations using the cohesive zone model", *J. Petrol. Sci. Eng.*, **165**, 42-57. https://doi.org/10.1016/j.petrol.2018.01.063.
Wang, B., Wu, C., Kang, L.G., Reniers, G. and Huang, L. (2018), "Work safety in China's thirteenth five-year plan period (2016–2020): Current status, new challenges and future tasks", *Safety Sci.*, **104**, 164-178. https://doi.org/10.1016/j.ssci.2018.01.012.
Wu, Q., Liu, Y., Wu, X., Liu, S., Sun, W. and Zeng, Y. (2016), "Assessment of groundwater inrush from underlying aquifers in Tunbai coal mine, Shanxi province, China", *Environ. Earth Sci.*, **75**(7379). https://doi.org/10.1007/s12665-016-5542-4.
Yao, Q.L. (2011), "Researches on strength weakening mechanism and control of water-enriched roofs of roadway", Ph.D. Dissertation, China University of Mining and Technology, Xuzhou, China.
Yasuhara, H., Kinoshita, N., Ohfuji, H., Lee, D.S., Nakashima, S. and Kishida, K. (2011), "Temporal alteration of fracture permeability in granite under hydrothermal conditions and its interpretation by coupled chemo-mechanical model", *Appl. Geochem.*, **26**(12), 2074-2088. https://doi.org/10.1016/j.apgeochem.2011.07.005.
Zhang, Q. (2020), "Hydromechanical modeling of solid deformation and fluid flow in the transversely isotropic fissured rocks", *Comput. Geotech.*, **128**, 103812. https://doi.org/10.1016/j.compgeo.2020.103812.
Zhang, Q., Yan, X. and Shao, J. (2021), "Fluid flow through anisotropic and deformable double porosity media with ultra-low matrix permeability: A continuum framework", *J. Petrol. Sci. Eng.*, **200**, 108349. https://doi.org/10.1016/j.petrol.2021.108349.
Zhao, C., Jin, D., Geng, J. and Sun, Q. (2019a), "Numerical simulation of the groundwater system for mining shallow buried coal seams in the ecologically fragile areas of Western China", *Mine Water Environ.*, **38**(1), 158-165. https://doi.org/10.1007/s10230-018-0551-z.
Zhao, C., Jin, D., Wang, H., Wang, Q., Wang, S. and Liu, Y. (2019b), "Construction and application of overburden damage and aquifer water loss model in medium-deep buried coal seam mining in Yushen mining area", *J. China Coal Soc.*, **44**(7), 2227-2235. https://doi.org/10.13225/j.cnki.jccs.2019.0159.
Zhao, J.H., Zhang, X.G., Jiang, N., Yin, L.M. and Guo, W.J. (2020a), "Porosity zoning characteristics of fault floor under fluid-solid coupling", *B. Eng. Geol. Environ.*, **78**(8), 6267-6283. https://doi.org/10.1007/s10064-019-01508-z.
Zhao, Y., Wu, Q., Chen, T., Zhang, X., Du, Y. and Yao, Y. (2020b), "Location and flux discrimination of water inrush using its spreading process in underground coal mine", *Safety Sci.*, **124**, 104566. https://doi.org/10.1016/j.ssci.2019.104566.
Zhou, F., Sun, W., Shao, J., Kong, L. and Geng, X. (2020), "Experimental study on nano silica modified cement base grouting reinforcement materials", *Geomech. Eng.*, **20**(1), 67-73. https://doi.org/10.12989/gae.2020.20.1.067.

CC